Structural Stability and Dynamics of an Amyloid-Forming Peptide GNNQQNY from the Yeast Prion Sup-35

Jie Zheng,* Buyong Ma,* Chung-Jung Tsai,* and Ruth Nussinov*†
*Basic Research Program, SAIC-Frederick, Center for Cancer Research Nanobiology Program, NCI-Frederick, Frederick, Maryland; and †Sackler Institute of Molecular Medicine, Department of Human Genetics and Molecular Medicine, Sackler School of Medicine, Tel Aviv University, Tel Aviv, Israel

ABSTRACT A seven amino acid yeast prion sup-35 fragment (GNNQQNY) forms amyloid fibrils. The availability of its detailed atomic oligomeric structure makes it a good model for studying the early stage of aggregation. Here we perform long all-atom explicit solvent molecular simulations of various sizes and arrangements of oligomer seeds of the wild-type and its mutants to study its stability and dynamics. Previous studies have suggested that the early stage rate-limiting step of oligomer formation occurs in high-order oligomers. Our simulations show that with the increase in the number of strands even from a dimer to a trimer, oligomer stability increases dramatically. This suggests that the minimal nucleus seed for GNNQQNY fibril formation could be small and is likely three or four peptides, in agreement with experiment, and that higher-order oligomers do not dissociate quickly since they have small diffusion coefficients and thus slow kinetics. Further, for the hydrophilic polar GNNQQNY, there are no hydrogen bonds and no hydrophobic interactions between adjacent β-sheets. Simulations suggest that within the sheet, the driving forces to associate and stabilize are interstrand backbone-backbone and side chain-side chain hydrogen bonds, whereas between the sheets, shape-complementary by the dry polar steric zipper via the side chains of Asn-2, Gln-4, and Asn-6 holds the sheets together, as proposed in an earlier study. Since the polar side chains of Asn-2, Gln-4, and Asn-6 act as a hook to bind two neighboring sheets together, these geometric restraints reduce the conformational search for the correct side chain packing to a two-dimensional problem of intersheet side chain interactions. Mutant simulations show that substitution of Asn-2, Gln-4, or Asn-6 by Ala would disrupt this steric zipper, leading to unstable oligomers.

INTRODUCTION

Many proteins/peptides, even including those disease-unrelated, have an intrinsic potential to form highly ordered amyloid fibrils under appropriate conditions (1). These amyloidogenic proteins do not share sequence similarity or structural homology. Nevertheless, experimental evidence shows that amyloid fibrils adopt similar cross-β-sheet structures in which the β-sheets are parallel to the fibril axis and the β-strands within a sheet are perpendicular to the fibril axis. These findings imply that a general principle may govern amyloid fibril formation (2). Recent experiments have shown that soluble oligomeric intermediates are more toxic than fully formed mature amyloid fibrils (3–5), implying that soluble oligomers, rather than insoluble fibrils, may be regarded as the primary toxic species of amyloids. Yet, despite the efforts and the progress which have been made, the mechanism of amyloid formation and the origin of its toxicity are still not fully understood.

Both experimental and theoretical studies have been extensively performed to elucidate protein aggregation. Due to the noncrystalline and insoluble nature of the amyloid fibrils, it is difficult to obtain atomic-resolution structures for amyloid fibrils in aqueous solution using traditional experimental methods, such as x-ray crystallography and nuclear magnetic resonance (NMR). Recently, solid state NMR has been used extensively on a number of systems, providing insights into the structural organization for both short peptide oligomers and oligomers of the entire Aβ. Tycko and co-workers (6,7) proposed a structural model for Aβ_{1-40} fibrils, in which an in-register parallel β-sheet was formed, with each peptide comprised of a β-strand (residues 12–24), a tight turn (residues 25–29), and another β-strand (residue 30–40). Similar bent double-layered hairpin-like structure for the Aβ_{1-40} was independently predicted by Ma and Nussinov (8) using molecular dynamics (MD) simulations. Lührs et al. (9) have recently determined a three-dimensional structure of Aβ_{1-42} fibrils using hydrogen-bonding constraints from quenched hydrogen/deuterium-exchange NMR. Computationally, amyloid formation has often been studied by examining the structural stability of the amyloid state alone using all-atom MD simulations with explicit solvent. These simulations mainly focus on finding the thermodynamically most stable conformation. Ma and Nussinov (8) performed a series of high-temperature MD simulations to examine different possible β-sheet arrangements of Aβ oligomers. Simulation results showed that an antiparallel β-sheet orientation is the most stable conformation for the Aβ_{16-22}. Zanuy et al. (10,11) reported that NFGAIL peptides adopt an antiparallel orientation within the sheets and parallel organization between sheets using the protocol proposed by Ma and Nussinov (8). These studies have shown that, for this class of peptides, the driving force is the hydrophobic interactions. However, the hydrophobic effect is not always

Submitted February 16, 2006, and accepted for publication April 25, 2006.
Address reprint requests to R. Nussinov, NCI-Frederick, 469-151 CCRNP, Frederick, MD 21702. Tel.: 301-846-5579; Fax: 301-846-5598; E-mail: ruthn@ncifcrf.gov.

0006-3495/06/08/824/10 $2.00
doi: 10.1529/biophysj.106.083246

necessary for amyloid aggregation since some hydrophilic peptides can also form ordered amyloids (12,13). Tsai et al. (14,15) carried out constant-temperature MD and parallel-tempering MD (PTMD) simulations to study the stability and energy landscape of the hydrophilic peptide DFNKF. They found that the most stable organization of the DFNKF oligomers is a parallel β-stranded sheet. The β-sheets are stabilized by both backbone-backbone and side chain-side chain hydrogen bonding to a large extent due to Asn-Asn stacking. An alternative way of studying amyloid formation is to directly investigate the transition pathways between random coil, α-helix, or pre-formed β sheet and β-sheet amyloid states at the very early stage. Since the formation of amyloid fibrils from peptide self-assembly is a slow process on the timescale of minutes to days (5), which is typically beyond the timescale of nanoseconds for classical all-atom MD simulations, these simulations employed either simplified models such as coarse-grained and lattice models or implicit solvent or both, to overcome the timescale problem. Nguyen and Hall (16) and Urbanc et al. (17) employed discontinuous molecular dynamics (DMD) with a coarse-grained protein model in implicit solvent to simulate spontaneous fibril formation of polyalanine and Aβ peptides, respectively. The modeling suggested that both hydrophobic interactions and protein geometry play an important role in the fibril formation.

In this work, we performed all-atom MD simulations to study the structural stability and dynamics of GNNQQNY peptides in explicit water. One-sheet and two-sheet models with parallel strands within the sheets and antiparallel organization between sheets were considered. Six specific alanine mutant simulations were also conducted to examine sequence effects. The GNNQQNY peptide was chosen for this study for a number of reasons: First, Eisenberg and co-workers (18) have recently determined the first crystal structure of the GNNQQNY from the yeast protein Sup-35 by x-ray microcrystallography. This atomic-resolution crystal structure of GNNQQNY makes it possible to investigate the mechanism of amyloid formation by molecular modeling methods and directly compare the modeling with experimental results. Second, Eisenberg et al. found that the GNNQQNY peptides exhibit similar amyloid properties as the entire Sup-35, including cooperative kinetics of aggregation, fibril formation, binding of the dye Congo red, and the characteristic cross-β x-ray diffraction pattern (12). This indicates that the study of short peptide aggregation could illustrate some common fundamental mechanism that governs fibril formation in large protein systems. Third, the small size of GNNQQNY peptide is highly amenable to atomistic simulations, which allow us to extensively examine different systems in reasonable computational time. Hence, this short seven-residue sequence, GNNQQNY, is a good model for studying the early stage in the aggregation process. This stability study can shed light on possible mechanisms of fibrillogenesis.

RESULTS

Unless otherwise indicated, all simulation systems have an organization of parallel strands within the sheets (both one-sheet and two-sheet models) and antiparallel orientation between the sheets (for two-sheet models), consistent with the x-ray observations (18). For clarity and convenience, the relationship among oligomer, β-sheet, and β-strand is that the oligomer is composed of β-sheets, whereas the β-sheet is composed of β-strands. A summary of the simulations is provided in Table 1.

The stability of the GNNQQNY oligomers

Six wild-type simulations (models A1–A6) were conducted for antiparallel β-sheets with parallel strands within the sheets. The relative stability of peptides in the model systems is measured by the backbone root mean-squared deviation (RMSD). The intra- and intersheet interactions are indicated by native contacts consisting of backbone hydrogen bonds and side chain contacts (14). A hydrogen bond is assigned if the distance between donor D and acceptor A is ≤ 3.6 Å and the angle D–H...A is $\geq 120°$ and a side chain contact is defined if the distance between the center of mass of two adjacent side chains is <6.7 Å. The reference structure for calculating backbone RMSD and the percentage of native contacts is the energy-minimized crystal structure. As shown in Fig. 1 *a*, for the model systems of A2, A3, A5, and A6, the RMSDs were maintained at 2.6 ± 0.3 Å within 10 ns, indicating significant stability of the structures. For the model systems of A1 (one two-stranded sheet) and A4 (two two-stranded sheets), the RMSDs showed large fluctuations within the first 4 ns and then increased quickly to $\sim$7 Å after 6 ns, which indicated that they lost their original dimer organization. Fig. 1 *b* shows that stable systems (A2, A3, A5, and A6) maintained at least 95% of their native contacts, whereas unstable systems (A1 and A4) significantly lost 50% and 90% of the native contacts after $\sim$6 ns, respectively. The correlation between the stability of the oligomers and the native contacts suggests that the intra- and intersheet interactions play an important role in stabilizing the oligomers. As shown in Fig. 2 *a*, the residue-based RMSDs indicate that all structures have common characteristics of small RMSDs for the five central residues whereas large RMSDs for the two end residues, indicating that the two residues at the termini are more flexible than the residues in the central regions. For the dimeric structures (models A1 and A4), since all chains were located at the edge of the oligomers (i.e., more exposed to the solvent), the flexibility of the residues in the central regions increased dramatically. Analysis of the number of hydrogen bonds of individual residues (Fig. 2 *b*), averaged from 10 ns simulations, showed that the average number of hydrogen bonds for the central residues is larger than those for the two end residues for all cases, consistent with the residue-based RMSD results. The larger

TABLE 1 Summary of simulation conditions at 330 K

	Systems	Strand/sheet organization	Simulation box size (Å)	Times (ns)
Wild-type				
A1	One sheet, two strands	Parallel/ –	38 × 28 × 30	10
A2	One sheet, three strands	Parallel/ –	38 × 33 × 30	10
A3	One sheet, four strands	Parallel/ –	38 × 38 × 30	10
A4	Two sheets, two strands	Parallel/antiparallel	40 × 30 × 38	10
A5	Two sheets, three strands	Parallel/antiparallel	40 × 35 × 38	10
A6*	Two sheets, four strands	Parallel/antiparallel	40 × 40 × 38	10
A7¶	Two sheets, four strands	Parallel/parallel	40 × 40 × 38	5
Mutants				
B1	Two sheets, four strands, N2A	Parallel/antiparallel	40 × 40 × 38	10
B2	Two sheets, four strands, N3A	Parallel/antiparallel	40 × 40 × 38	10
B3	Two sheets, four strands, Q4A	Parallel/antiparallel	40 × 40 × 38	10
B4	Two sheets, four strands, Q5A	Parallel/antiparallel	40 × 40 × 38	10
B5	Two sheets, four strands, N6A	Parallel/antiparallel	40 × 40 × 38	10
B6	Two sheets, four strands, Y7A	Parallel/antiparallel	40 × 40 × 38	10

Models of A1–A3 consist of two, three, and four parallel strands in a single sheet, respectively.
Models of A4–A6 consist of two two-, three-, and four-parallel-strands sheets, with the sheets arranged in an antiparallel fashion with respect to each other. Model A7 consists of two four-parallel-stranded sheets, with the sheets arranged in parallel.
Models of B1–B6 consist of two four-parallel-stranded sheets, with the sheets arranged in an antiparallel fashion with respect to each other. The specific mutation sequences, corresponding to B1–B6, are G**A**NQQNY, GN**A**QQNY, GNN**A**QNY, GNNQ**A**NY, GNNQQ**A**Y, GNNQQN**A**.
*Schematic organization of a tetramer model of A6.
¶Schematic organization of a tetramer model of A7.

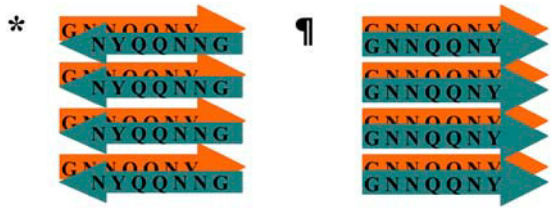

residue-based RMSDs of the two termini residues were due to the reduction of hydrogen bonds between the peptides. The side chains of the termini residues are more exposed to the water and tend to form hydrogen bonds with water molecules rather than peptides. The hydrogen bonds between the two end residues (Gly-1 and Tyr-7) and water molecules are weak and easily break and reform within very short time periods. It should be noted that the end residue Tyr-7 has a larger number of hydrogen bonds and smaller RMSD than the other end residue, Gly-1. This is due to the stacking of aromatic rings of the residues Tyr-7. The aromatic rings were stacked on top of each other (Fig. 3), thus providing strong π-π-interactions stabilizing the GNNQQNY oligomers. Trebbi and co-workers (19) recently found that aromatic clusters of Tyr, Trp, and Phe residues that had significant low-frequency motion can promote protein stability due to the favorable entropic contribution. Fig. 3 presents a typical snapshot of the hydrogen bonding between backbone-backbone and side chain-side chain taken from two four-stranded sheets (model A6) at 10 ns. Within the sheets, each GNNQQNY peptide has ~7 backbone-backbone hydrogen bonds and ~6 side chain-side chain hydrogen bonds with its neighboring peptides. Those hydrogen bonds were almost evenly distributed along the peptide, allowing them to stabilize the in-register β-structures. Between the sheets, no hydrogen bonds were observed, in agreement with experimental observations (18).

To further examine the structural organization of the peptides, interstrand (d_{strand}) and intersheet (d_{sheet}) distances were used to characterize the peptide associations. The d_{strand} is calculated by averaging the mass center distance between each residue in one strand and its corresponding residue in the adjacent strand in the same sheet, whereas d_{sheet} is calculated by averaging the mass center distance between each strand in one sheet and its corresponding strand in the adjacent sheet (see Fig. 4 *a* for the detailed mathematical expressions). As shown in Fig. 4, *b–c*, two dimeric systems (A1 and A4) can not preserve both the interstrand and intersheet distances during the 10 ns simulations, whereas the other four models (A2, A3, A5, and A6) were able to maintain the interstrand distance of 4.8 ± 0.3 Å and the intersheet distance of 8.7 ± 0.2 Å throughout the simulations. The interstrand distance in the A4 system with double sheets was retained at its initial distance a little longer than that of the A1 system with a single sheet. After ~6 ns, both A1 and A4 totally lost their original integrity. It appears that an extra sheet could delay the progressive loss of the β-structural organization. In the case of the A4 system, intrasheet and intersheet dissociations occur almost at the same time due to the loss of hydrogen bonding within sheets and side chain contacts between sheets.

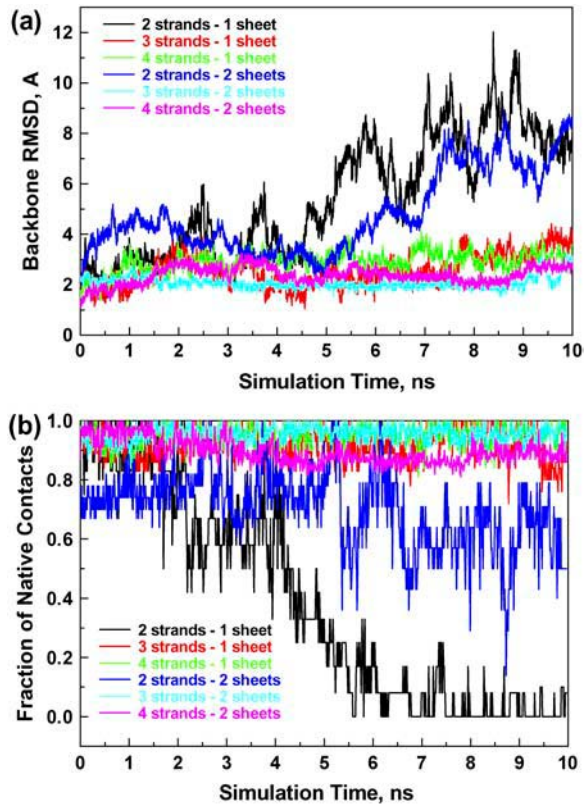

FIGURE 1 Simulations of the wild-type models of A1–A6. (*a*) RMSD of the backbone atoms and (*b*) the fraction of native contacts, with respect to the minimized crystal structure as a function of time. The color code is as follows (see Table 1): black, A1; red, A2; green, A3; blue, A4; cyan, A5; and purple, A6.

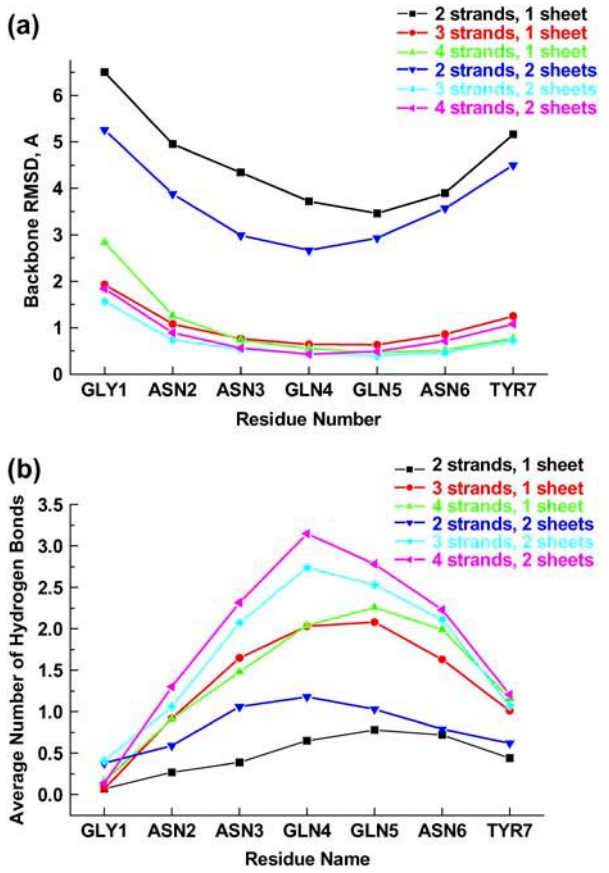

FIGURE 2 Simulations of the wild-type models of A1–A6. (*a*) Average residue-based RMSD of the backbone atoms and (*b*) average number of hydrogen bonds for individual residues.

To probe the geometrical π-stacking of Tyr residues of the oligomers, we examined the Tyr side chain orientation by constructing an end-to-end vector connecting the side chain carbon atom C_β to the side chain oxygen atom OH. For each pair of adjacent Tyr side chains, a scalar product between the end-to-end vectors of each side chain was calculated: 1 indicates parallel, -1 antiparallel, and 0 perpendicular to each other. As seen in Fig. 6 *a*, for the models of A2, A3, A5, and A6, the Tyr aromatic rings were well packed in a parallel fashion with the mass center distance between two adjacent Tyr side chains ~5–5.5 Å throughout the 10 ns simulations, whereas for the models of A1 and A4, they lost their original parallel aromatic ring stacking very quickly, leading to the unstable oligomers.

In addition, to examine possible molecular packing between sheets, we performed additional MD simulation (model A7) of the octamers with parallel sheets and four parallel strands in each sheet. The RMSD value (Fig. 5 *a*) increased rapidly to 4 Å within ~250 ps and then gradually reached ~8 Å within 5 ns, indicating that the parallel octamers are unable to preserve their original organization, in agreement with experimental observations (18). The parallel-sheet organization is less stable than the antiparallel-sheet organization. The large decrease in stability of the parallel sheets could be mainly attributed to the loss of intra- and intersheet interactions as shown in Fig. 5 *b*. The loss of π-π interactions may also contribute to the stability of the oligomers (Fig. 6 *b*). It should be noted that even though the fraction of the native contacts was still maintained at ~70% during a 5-ns simulation, the secondary structure of the β-strands in one sheet was no longer preserved as shown in Fig. 5 *c*. The β-strands in one sheet first lost their parallel integrity and then dissociated from the other sheet.

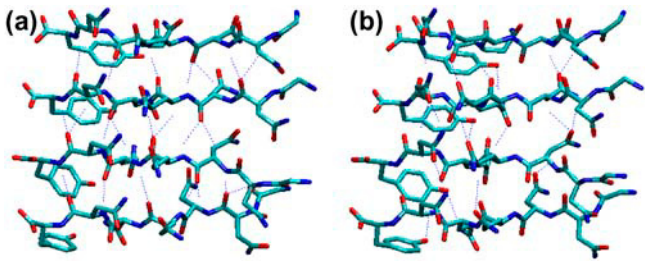

FIGURE 3 Model A6 (two four-stranded antiparallel sheets) is used here for illustration at 10 ns. One sheet is omitted for clarity. (*a*) Backbone-backbone hydrogen bonds; (*b*) Side chain-side chain hydrogen bonds.

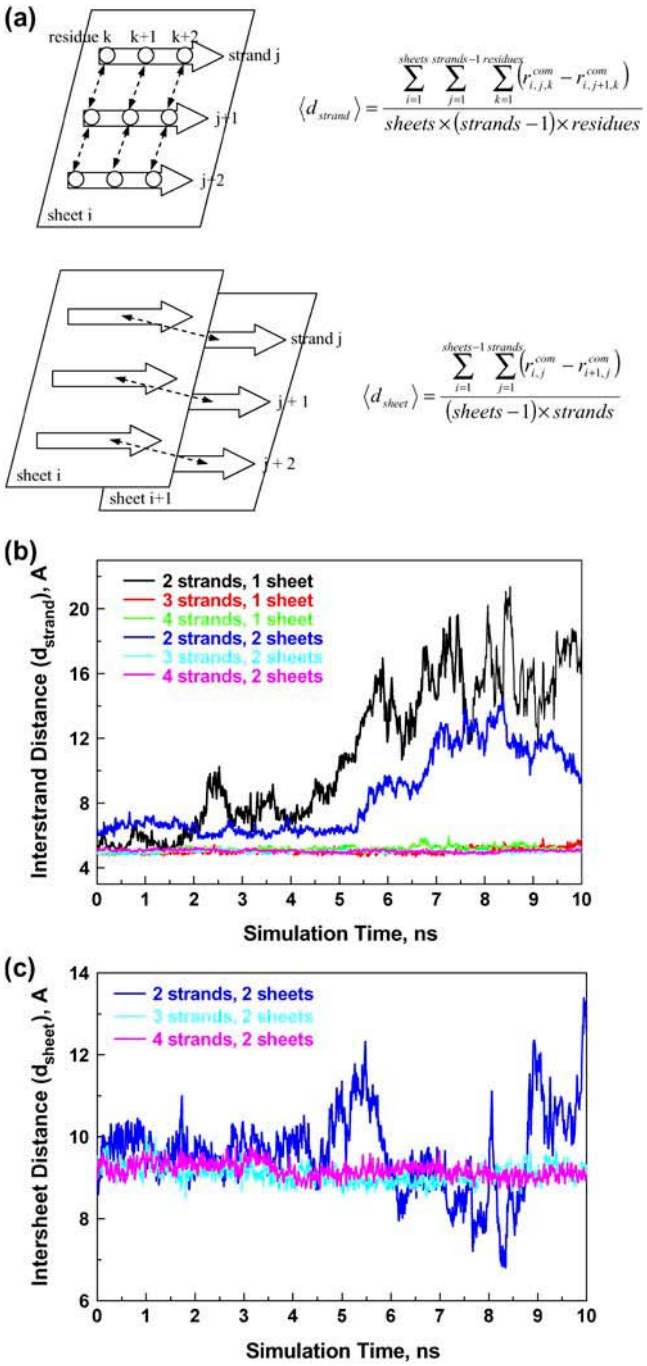

FIGURE 4 (*a*) Definition of geometrical parameters for characterizing the structural organization of models A1–A6. (*b*) The average distance between the center of mass of two neighboring strands. (*c*) The average distance between the center of mass of two neighboring sheets.

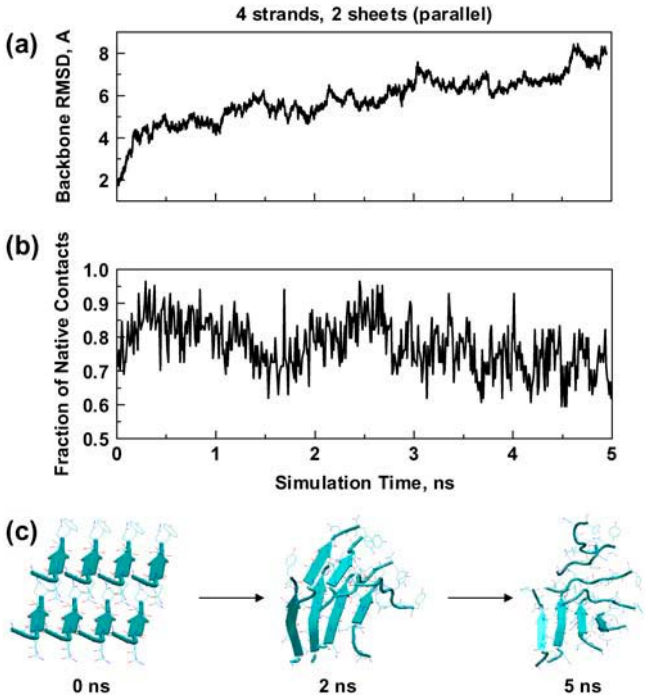

FIGURE 5 Simulation of the model A7. (*a*) RMSD of the backbone atoms; (*b*) the fraction of native contacts; and (*c*) Ssnapshots of the model A7, illustrating the disassociate evolution at 0, 2, and 5 ns.

The stability of mutant oligomers: sequence effects

To investigate the effect of mutations on the GNNQQNY stability, five central residues (Asn-2, Asn-3, Gln-4, Gln-5, and Asn-6) and one end residue (Tyr-7) of GNNQQNY were mutated to alanines. The mutant systems were simulated and compared to the wild-type GNNQQNY. Fig. 7 *a* shows the backbone RMSD over time for all mutants. As can be seen, none of the mutants was as structurally stable as the wild-type, indicating that the side chain interactions play an important role in determining the stability of the GNNQQNY oligomers. However, the N3A and Q5A mutants have small RMSD values (~2.5 Å), whereas the N2A, Q4A, N6A, and Y7A mutants have large RMSD values (>4.0 Å). Comparison between the dynamics of the wild-type and its mutants suggests that mutations N3A and Q5A have little effect on the structural stability of the GNNQQNY (low RMSD, large fraction of native contacts, and constant interstrand and intersheet distances), whereas mutations N2A, Q4A, N6A, and Y7A destabilize the oligomeric structures. The destabilization of the Q4A mutant is even more pronounced. A large twist angle (>15°) between the strands was observed for all the mutants. In Fig. 6 *c*, in the mutants N2A and N3A, the packing of aromatic rings was well maintained in a parallel fashion over the 10 ns trajectory. On the other hand, in the mutants Q4A, Q5A, and N6A, the orientation of the aromatic rings fluctuated between parallel and perpendicular. Fig. 8 shows the atomic structure of a two-sheet GNNQQNY and the sites of the mutations. As seen in Fig. 8, the polar side chains of residues Asn-2, Gln-4, and Asn-6 of two neighboring sheets were oriented toward the interface between the sheets, tightly hooking with each other, forming a steric zipper (12,18). Mutations of Asn-2, Gln-4, or Asn-6 to Ala would knock down this intersheet steric zipper, leading to

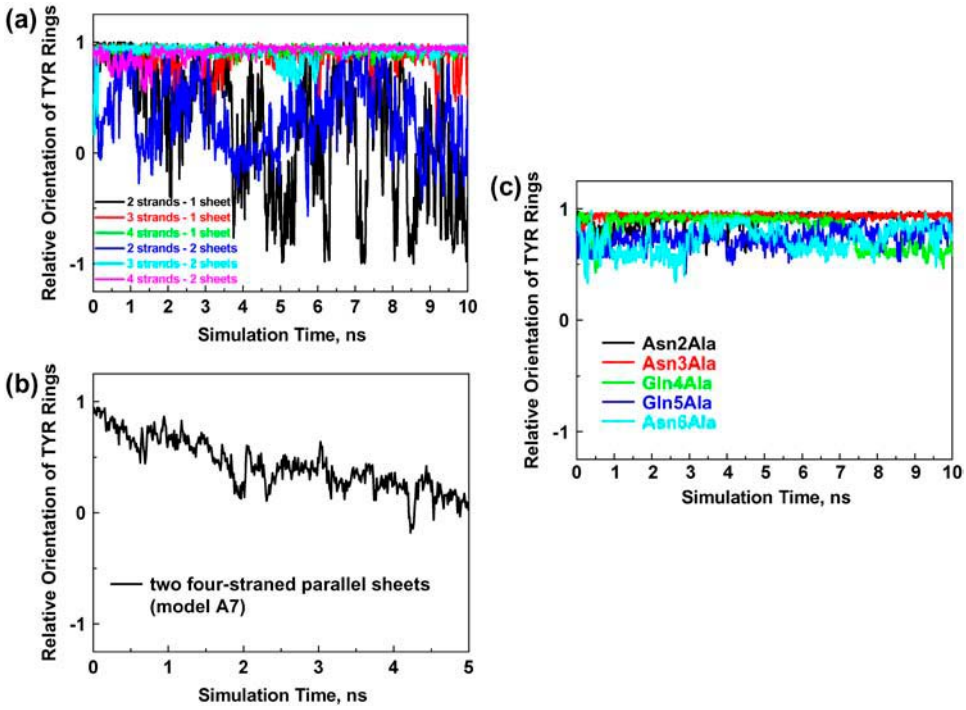

FIGURE 6 Relative orientation between the Tyr side chains where 1 indicates parallel, −1 antiparallel, and 0 perpendicular. (*a*) Wild-type models of A1–A6 with antiparallel β-sheets; (*b*) wild-type model of A7 with parallel β-sheets; and (*c*) mutant models of B1–B5 with antiparallel β-sheets.

destabilization of the oligomeric structures. This destabilization is due not only to changes in the side chain-side chain interactions but also to the loss of internal hydrogen bonds (Fig. 7 *b*). Water molecules do not penetrate into the interface between two neighboring sheets, in agreement with experiments (18). The strong association between neighboring sheets is accompanied by the release of water molecules from the sheet-sheet interface into the bulk water, which provides

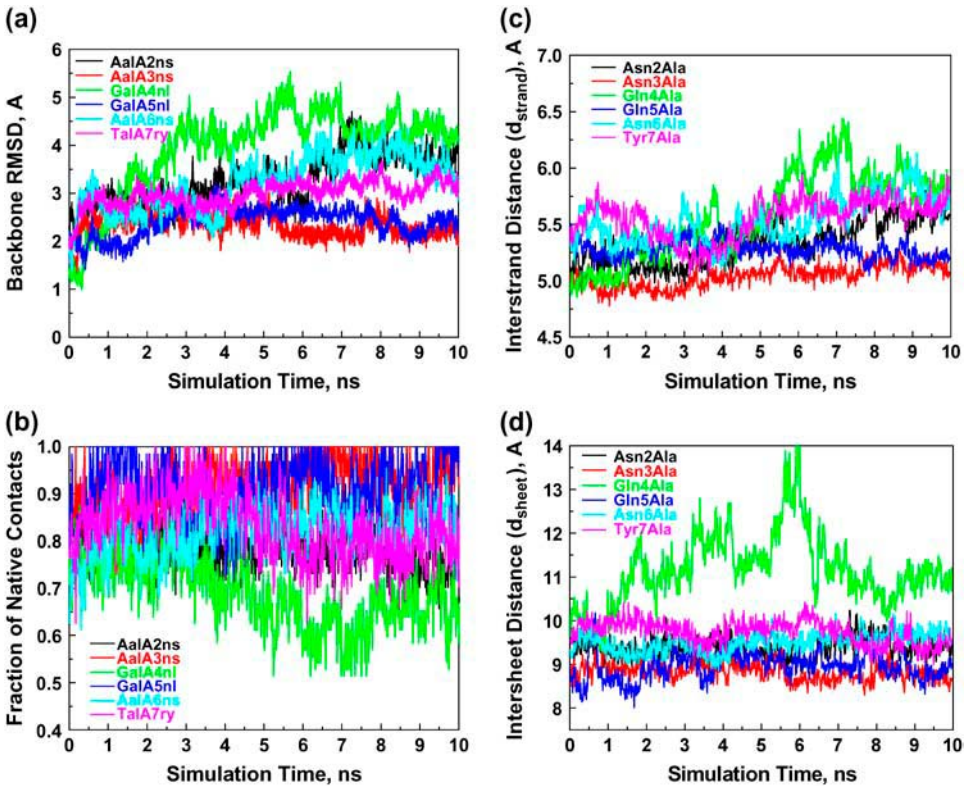

FIGURE 7 Simulation of mutant systems of B1–B6. (*a*) RMSD of the backbone atoms; (*b*) the fraction of native contacts; (*c*) The average distance between the center of mass of two neighboring strands; and (*d*) the average distance between the center of mass of two neighboring sheets.

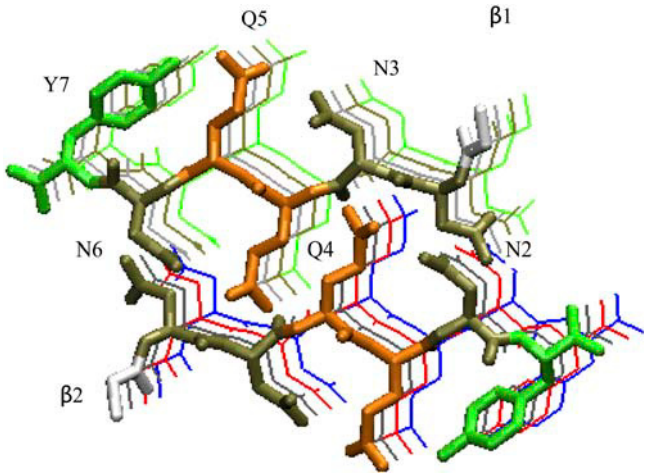

FIGURE 8 Intersheet steric zipper is formed between side chains of residues Asn-2, Gln-4, and Asn-6 of sheet β1 and those of the same residues of sheet β2. This octamer model is constructed using recent x-ray crystal coordinates (Protein Data Bank code 1YJP) (18).

a favorable entropic contribution to the free energy state. On the other hand, since the side chains of Asn-3 and Gln-5 point toward the peptide-water interface, Ala substitutions at those two positions did not alter the shape-complementary of the steric zipper. Thus these mutations still lead to relatively stable structures. It is important to note that, in the case of the mutation of the aromatic residue Tyr-7 to Ala, the octamer loses its original organization as indicated by the large RMSD and the large interstrand and intersheet distances. This large destablization could arise from the loss of π-π stacking interactions. The importance of aromatic residues in amyloidogenesis has been demonstrated in many other peptides (20).

DISCUSSION AND CONCLUSIONS

Amyloid formation is a dynamic process involving three basic steps: nucleation, monomer addition/oligomer aggregation, and fibril formation. The self-assembly process also requires the peptides to undergo complex conformational transition and reorganization between intermediates. The kinetics of fibril formation is still hotly debated and remains an important open question. Collins and co-workers (21) proposed a mechanism of amyloid formation based on the yeast prion protein Sup-35. They suggested that amyloid growth can occur by the addition of monomers to the existing oligomers. Petty et al. (22) and Silva et al. (23) proposed an alternative growth model, in which peptide strands aggregate rapidly to form disordered β-sheets which then rearrange themselves to ordered oligomers by two different competing mechanisms. At low concentration, the detachment-reattachment of one or more strands from/onto existing β-sheets dominates; at high concentration, peptides would slowly slide or diffuse within the β-sheets to adopt a more favorable alignment without detachment or reattachment of individual strand; at intermediate concentrations, both alignment mechanisms occur (23). Nevertheless, these simple nucleation-dependent polymerization models are still insufficient to describe all the aspects of the dynamic process of amyloid formation (24). Thus, determining the stable structure of the preformed oligomers in the first steps of the assembly process is important. MD simulations have been used to investigate the molecular properties of amyloid-forming peptides, complementing experiment. Even though conventional MD simulations do not explore the dynamic mechanism of amyloid fibril formation due to a huge timescale gap between simulations and experiments, here we solely focus on studying the dynamical behavior of the oligomeric structure and the factors determining the oligomeric stability.

In this work, MD simulations showed that wild-type oligomeric structures containing dimer conformations were unstable. These unstable dimer conformations may be the outcome of two possible reasons. First, the dimers in single sheet or double sheets are not the predominant species in solution. Similar unstable dimer structures were also observed in other amyloid-forming peptides. Bernstein et al. (25) found that no $A\beta_{1-42}$ dimers were observed by using mass spectrometry and ion mobility spectrometry. In simulations of $A\beta_{1-40}$ and of $A\beta_{1-42}$ fragments using free energy calculations, Urbanc et al. (26) and Wu et al. (27) observed that both $A\beta_{1-40}$ and $A\beta_{1-42}$ dimers are not thermodynamically stable. Second, there is a rapid interchange between dimers and monomers or higher-order oligomers. Several studies suggested that the rate-limiting step at the early stage of oligomer formation occurs in high-order oligomers (28). Our simulation results showed that with the increase in the number of strands even from dimer to trimer, the stability of the oligomers increased dramatically. This suggests that i), the minimal nucleus seed for GNNQQNY fibril formation could be small and is likely three or four peptides, in agreement with experimental data (18); and ii), higher-order oligomers do not dissociate quickly because the large oligomers have small diffusion coefficients and thus slow kinetics.

In highly hydrophobic peptides such as $A\beta_{16-22}$ (KLVF FAE), the Syrian hamster prion protein $(ShPrP)_{113-120}$ (AGAAAAGA), and the human islet amyloid $polypeptide_{22-27}$ (NFGAIL), hydrophobic attraction is a major driving force for stabilizing and aggregation of oligomers. But, for the hydrophilic polar GNNQQNY peptide, there are no hydrogen bonds and no hydrophobic interactions between the β-sheets. What is driving force to associate and stabilize the β-sheets? Simulation results show that within the sheet, interstrand backbone-backbone and side chain-side chain hydrogen bonds hold the strands together to form the ordered β-sheet, whereas between the sheets, shape-complementary by a steric zipper via the side chains of Asn-2, Gln-4, and Asn-6 holds the sheets together to form the oligomer. The central region of the peptides (N2–N5) has a larger number

of hydrogen bonds with longer residence times than the end residues, assisting in the formation and stabilization of the β-sheet. Since the polar side chains of Asn-2, Gln-4, and Asn-6 act as a hook to bind two neighboring sheets together, these geometric restraints reduce the conformational search for the correct side chain packing to a two-dimensional problem of intersheet side chain interactions (9). Mutant simulations showed that substitution of Asn-2, Gln-4, or Asn-6 by a shorter Ala residue would disrupt this steric zipper between two neighboring sheets. Substituted Ala may not adopt a favorable geometry with strong van der Waals interactions with its neighboring sheet. Consequently, the substantial reduction in the van der Waals intersheet interactions leads to destabilization of the oligomers. These results suggest that the correct geometrical matching of the side chains via intersheet interactions plays an important role in determining the stability of oligomers. Nelson et al. (18) also expected that a sequence similar to Asn-X-Gln-X-Asn can form a steric zipper, possibly leading to amyloid-like fibril. Gsponer et al. (29) and Lipfert et al. (30) emphasized the role of side chain interactions in the early aggregation steps of the peptide GNNQQNY by MD simulations. The π-π interactions between the aromatic rings may also have a large influence on amyloid formation and stabilization. Wild-type sequence simulations showed that the loss of parallel packing of the aromatic rings leads to unstable oligomers (e.g., models A1, A4, and A7). Similarly, mutant simulation in the absence of the Tyr ring also showed decreased stability. Gazit (31) found a significant high propensity of aromatic residues such as Phe, Tyr, and Trp in a variety of amyloid-related peptides. This finding suggested that π-stacking interactions have a key role in molecular recognition, self-assembly, and amyloid formation. Makin and co-workers (20) further confirmed that aromatic residues capable of π-π stacking were important for fibril formation. Highly conserved aromatic residues offer strong entropic contributions stabilizing existing oligomers/fibrils. Moreover, desolvation between neighboring sheets gains more entropic energy by releasing water molecules from peptide interfaces to the bulk solvent. In addition, Asn/aromatic-rich peptides were found to tend to aggregate and thus may serve as a common denominator for amyloid formation of various amyloidogenic peptides (15). Dobson (32) suggested that the interactions of the peptide or protein main chain, particularly hydrogen bonds, dominate other interactions in the amyloid core as they are common to all, and that the side chains affect the details of the assembly, not the general structural characteristics. However, it is clear that all amyloid fibrils exhibit similar cross-β-structure, with not only main chains aligned in a parallel/antiparallel fashion, but also side chains aligned along the fibril axis. This fact indicates that both main chain and side chain interactions are common in amyloids. Thus, for the hydrophilic polar GNNQQNY peptide, the hydrogen bonding of backbone-backbone and side chain-side chain (intrasheet interactions), specific side chain packing (intersheet interactions), and aromatic rings stacking (π-π interactions) are mainly responsible for the high stability of the oligomers. It should be pointed out that although this study provides useful insights into the structural stability and dynamics of different oligomeric arrangements, it does not explore the oligomerization process of the peptides due to the limitations of computer power and simulation methods. A complete description of the oligomer assembly will require further analysis using both advanced simulations with efficient sampling methods (e.g., the replica-exchange MD and coarse-grained mode model) and experiments.

Simulation methods

Model systems

The initial monomer structure of the GNNQQNY was taken from the x-ray crystal structure (18) (Protein Data Bank code 1YJP). For any given model, the initial strand-strand separation within sheets was set to 4.87 Å and sheet-sheet separation was set to 8.5 Å, corresponding to the experimental data (18). The strands were packed parallel to each other and no translation was applied to one strand relative to the other. It is generally accepted that more stable structures can be obtained by increasing the contacts between peptide interfaces. The sheets were packed in a way as to obtain large contacts at the sheet-sheet interface with the polar side chain contacts (Asn-2-Asn-2, Gln-4-Gln-4, Asn-6-Asn-6) between two adjacent β-sheets matching each other perfectly without any steric overlaps. For the wild-type systems, the one sheet models consisted of two-, three-, and four-parallel-strands, respectively. The two-sheet models consisted of two-, three-, and four-parallel-strands within the sheets while maintaining antiparallel organization between the sheets. For mutant systems, six single-point alanine mutations were considered, namely N2A, N3A, Q4A, Q5A, N6A, and Y7A. Mutant systems were built based on the wild-type octamers with antiparallel β-sheets. In addition, one system consisting of two four-parallel-stranded sheets with parallel-sheet organization was also taken into account to examine a possible packing pattern. All initial structures were built using the CHARMM program. All simulations were performed using the CHARMM c31b2 software (33) and the PARAM22 force field (34).

Simulation protocol

Each model system was solvated in a preequilibrated box of TIP3P water molecules extending at least 16 Å from any solute atom. This ensures that peptides do not interact with their images. Any water molecule that is close to the peptides within 2.0 Å was removed. Each system was initially minimized in energy for 4000 cycles using the conjugate gradient

algorithm to remove any bad contacts between molecules. Minimized systems were gradually heated from 50 K to 330 K with 50 K increments in short 50 ps MD runs with harmonical constraints on the backbone atoms of the peptides to allow relaxation of water molecules. The equilibrium MD runs were performed by another 50 ps without position restraints on the peptides before the production runs. We used the NVT ensemble in an orthorhombic box. The periodic boundary condition and minimum image convention were applied in the x, y, and z directions. Initial velocities were assigned with a Maxwell-Bolzmann distribution at 330K. The velocity Verlet method with a time step of 1 fs was used for the integration of Newton's equation. The system was maintained at a constant temperature of 330K using the Berendsen thermostat with a time constant of 0.1 ps. Any covalent bond associated with hydrogen atoms was constrained by the SHAKE algorithm with a geometric tolerance of 0.0001. The switch function was used to calculate VDW interactions between 8.0 and 10.0 Å. The force-shifting function was used for the long-range electrostatic interactions at a cutoff distance of 12 Å. The atom-based force-shifting function and the particle-mesh Ewald technique generated stable and very similar nanosecond trajectories for double-stranded DNAs, proteins, and peptides (35,36). The cell-based neighbor list with a cutoff range of 13.2 Å was used to reduce the computational time for energy and energy-derivative calculations, which typically consume ~90% of the computational time. The nonbonded neighbor list was updated automatically if any atom in the list was moved by more than $(13.2 - 12)/2 = 0.6$ Å. All simulations were 5~10 ns long depending on the stability of the peptides and configurations were saved every 1.0 ps for analysis. All simulations were performed on a 22-node Linux cluster Intel x86.

We thank David Eisenberg for his interest in the ideas and results obtained in this work.

This project has been funded in whole or in part by federal funds from the National Cancer Institute, National Institutes of Health, under contract number NO1-CO-12400. This research was supported (in part) by the Intramural Research Program of the NIH, National Cancer Institute, Center for Cancer Research. This study utilized the high-performance computational capabilities of the Biowulf PC/Linux cluster at the National Institutes of Health, Bethesda, MD (http://biowulf.nih.gov).

The content of this publication does not necessarily reflect the views or policies of the Department of Health and Human Services, nor does mention of trade names, commercial products, or organizations imply endorsement by the U.S. Government.

REFERENCES

1. Plakoutsi, G., F. Bemporad, M. Calamai, N. Taddei, C. M. Dobson, and F. Chiti. 2005. Evidence for a mechanism of amyloid formation involving molecular reorganisation within native-like precursor aggregates. *J. Mol. Biol.* 351:910–922.
2. Thirumalai, D., D. K. Klimov, and R. I. Dima. 2003. Emerging ideas on the molecular basis of protein and peptide aggregation. *Curr. Opin. Struct. Biol.* 13:146–159.
3. Klein, W. L., J. W. B. Stine, and D. B. Teplow. 2004. Small assemblies of unmodified amyloid β-protein are the proximate neurotoxin in Alzheimer's diease. *Neurobiol. Aging.* 25:569–580.
4. Bucciantini, M., E. Giannoni, F. Chiti, F. Baroni, L. Formigli, J. Zurdo, N. Taddei, G. Ramponi, C. M. Dobson, and M. Stefani. 2002. Inherent toxicity of aggregates implies a common mechanism for protein misfolding diseases. *Nature.* 416:507–511.
5. Kayed, R., E. Head, J. L. Thompson, T. M. McIntire, S. C. Milton, C. W. Cotman, and C. G. Glabe. 2003. Common structure of soluble amyloid oligomers implies common mechanism of pathogenesis. *Science.* 300:486–489.
6. Petkova, A. T., Y. Ishii, J. J. Balbach, O. N. Antzutkin, R. D. Leapman, F. Delaglio, and R. Tycko. 2002. A structural model for Alzheimer's beta-amyloid fibrils based on experimental constraints from solid state NMR. *Proc. Natl. Acad. Sci. USA.* 99:16742–16747.
7. Tycko, R. 2004. Progress towards a molecular-level structural understanding of amyloid fibrils. *Curr. Opin. Struct. Biol.* 14:96–103.
8. Ma, B., and R. Nussinov. 2002. Stabilities and conformations of Alzheimer's beta-amyloid peptide oligomers (Abeta 16–22, Abeta 16–35, and Abeta 10–35): sequence effects. *Proc. Natl. Acad. Sci. USA.* 99: 14126–14131.
9. Luhrs, T., C. Ritter, M. Adrian, D. Riek-Loher, B. Bohrmann, H. Dobeli, D. Schubert, and R. Riek. 2005. 3D structure of Alzheimer's amyloid-{beta}(1–42) fibrils. *Proc. Natl. Acad. Sci. USA.* 102:17342–17347.
10. Zanuy, D., B. Ma, and R. Nussinov. 2003. Short peptide amyloid organization: stabilities and conformations of the islet amyloid peptide NFGAIL. *Biophys. J.* 84:1884–1894.
11. Zanuy, D., Y. Porat, E. Gazit, and R. Nussinov. 2004. Peptide sequence and amyloid formation: molecular simulations and experimental study of a human islet amyloid polypeptide fragment and its analogs. *Structure.* 12:439–455.
12. Balbirnie, M., R. Grothe, and D. S. Eisenberg. 2001. An amyloid-forming peptide from the yeast prion Sup35 reveals a dehydrated beta-sheet structure for amyloid. *Proc. Natl. Acad. Sci. USA.* 98:2375–2380.
13. Reches, M., Y. Porat, and E. Gazit. 2002. Amyloid fibril formation by pentapeptide and tetrapeptide fragments of human calcitonin. *J. Biol. Chem.* 277:35475–35480.
14. Tsai, H.-H., D. Zanuy, N. Haspel, K. Gunasekaran, B. Ma, C.-J. Tsai, and R. Nussinov. 2004. The stability and dynamics of the human calcitonin amyloid peptide DFNKF. *Biophys. J.* 87:146–158.
15. Tsai, H.-H., M. Reches, C.-J. Tsai, K. Gunasekaran, E. Gazit, and R. Nussinov. 2005. Energy landscape of amyloidogenic peptide oligomerization by parallel-tempering molecular dynamics simulation: significant role of Asn ladder. *Proc. Natl. Acad. Sci. USA.* 102:8174–8179.
16. Nguyen, H. D., and C. K. Hall. 2004. Molecular dynamics simulations of spontaneous fibril formation by random-coil peptides. *Proc. Natl. Acad. Sci. USA.* 101:16180–16185.
17. Urbanc, B., L. Cruz, S. Yun, S. V. Buldyrev, G. Bitan, D. B. Teplow, and H. E. Stanley. 2004. In silico study of amyloid {beta}-protein folding and oligomerization. *Proc. Natl. Acad. Sci. USA.* 101:17345–17350.
18. Nelson, R., M. R. Sawaya, M. Balbirnie, A. O. Madsen, C. Riekel, R. Grothe, and D. Eisenberg. 2005. Structure of the cross-beta spine of amyloid-like fibrils. *Nature.* 435:773–778.
19. Trebbi, B., F. Dehez, P. W. Fowler, and F. Zerbetto. 2005. Favorable entropy of aromatic clusters in thermophilic proteins. *J. Phys. Chem. B.* 109:18184–18188.
20. Makin, O. S., E. Atkins, P. Sikorski, J. Johansson, and L. C. Serpell. 2005. Molecular basis for amyloid fibril formation and stability. *Proc. Natl. Acad. Sci. USA.* 102:315–320.
21. Collins, S. R., A. Douglass, R. D. Vale, and J. S. Weissman. 2004. Mechanism of prion propagation: amyloid growth occurs by monomer addition. *PLoS Biol.* 2:1583–1590.

22. Petty, S. A., and S. M. Decatur. 2005. Experimental evidence for the reorganization of beta-strands within aggregates of the Abeta(16–22) peptide. *J. Am. Chem. Soc.* 127:13488–13489.

23. Silva, R. A. G. D., W. Barber-Armstrong, and S. M. Decatur. 2003. The organization and assembly of a beta-sheet formed by a prion peptide in solution: an isotope-edited FTIR study. *J. Am. Chem. Soc.* 125:13674–13675.

24. Bitan, G., A. Lomakin, and D. B. Teplow. 2001. Amyloid beta -protein oligomerization: prenuclation interactions revealed by photo-induced cross-linking of unmodified proteins. *J. Biol. Chem.* 276:35176–35184.

25. Bernstein, S. L., T. Wyttenbach, A. Baumketner, J. E. Shea, G. Bitan, D. B. Teplow, and M. T. Bowers. 2005. Amyloid beta-protein: monomer structure and early aggregation states of Abeta42 and its pro alloform. *J. Am. Chem. Soc.* 127:2075–2084.

26. Urbanc, B., L. Cruz, F. Ding, D. Sammond, S. Khare, S. V. Buldyrev, H. E. Stanley, and N. V. Dokholyan. 2004. Molecular dynamics simulation of amyloid beta dimer formation. *Biophys. J.* 87:2310–2321.

27. Wu, C., H. Lei, and Y. Duan. 2004. Formation of partially ordered oligomers of amyloidogenic hexapeptide (NFGAIL) in aqueous solution observed in molecular dynamics simulations. *Biophys. J.* 87:3000–3009.

28. Petty, S. A., and S. M. Decatur. 2005. Intersheet rearrangement of polypeptides during nucleation of {beta}-sheet aggregates. *Proc. Natl. Acad. Sci. USA.* 102:14272–14277.

29. Gsponer, J., U. Haberthur, and A. Caflisch. 2003. The role of side-chain interactions in the early steps of aggregation: molecular dynamics simulations of an amyloid-forming peptide from the yeast prion Sup35. *Proc. Natl. Acad. Sci. USA.* 100:5154–5159.

30. Lipfert, J., J. Franklin, F. Wu, and S. Doniach. 2005. Protein misfolding and amyloid formation for the peptide GNNQQNY from yeast prion protein Sup35: simulation by reaction path annealing. *J. Mol. Biol.* 349:648–658.

31. Gazit, E. 2002. A possible role for pi-stacking in the self-assembly of amyloid fibrils. *FASEB J.* 16:77–83.

32. Dobson, C. M. 2004. Principles of protein folding, misfolding and aggregation. *Semin. Cell Dev. Biol.* 15:3–16.

33. Brooks, B. R., R. E. Bruccoleri, B. D. Olafson, D. J. States, S. Swarminathan, and M. Karplus. 1983. CHARMM - a program for macromolecular energy, minimization, and dynamics calculations. *J. Comput. Chem.* 4:187–217.

34. MacKerell, A. D., D. Bashford, M. Bellott, R. L. Dunbrack, J. D. Evanseck, M. J. Field, S. Fischer, J. Gao, H. Guo, S. Ha, D. Joseph-McCarthy, L. Kuchnir, K. Kuczera, F. T. K. Lau, C. Mattos, S. Michnick, T. Ngo, D. T. Nguyen, B. Prodhom, W. E. Reiher, B. Roux, M. Schlenkrich, J. C. Smith, R. Stote, J. Straub, M. Watanabe, J. Wiorkiewicz-Kuczera, D. Yin, and M. Karplus. 1998. All-atom empirical potential for molecular modeling and dynamics studies of proteins. *J. Phys. Chem. B.* 102:3586–3616.

35. Beck, D. A. C., R. S. Armen, and V. Daggett. 2005. Cutoff size need not strongly influence molecular dynamics results for solvated polypeptides. *Biochemistry.* 44:609–616.

36. Steinbach, P. J., and B. R. Brooks. 1994. New spherical-cutoff methods for long-range forces in macromolecular simulation. *J. Comput. Chem.* 15:667–683.